On High Precipitation in Mozambique, Zimbabwe, and Zambia in February 2018

NEVEN S. FUČKAR, FRIEDERIKE E. L. OTTO, FLAVIO LEHNER, IZIDINE PINTO, EMMA HOWARD, SARAH SPARROW, SIHAN LI, AND DAVID WALLOM

AFFILIATIONS:

Fučkar—Environmental Change Institute, University of Oxford, Oxford, United Kingdom, and Earth Sciences Department, Barcelona Supercomputing Center, Barcelona, Spain;

Otto—Environmental Change Institute, University of Oxford, Oxford, United Kingdom;

Lehner—Climate and Global Dynamics Laboratory, National Center for Atmospheric Research, Boulder, Colorado;

Pinto—Climate System Analysis Group, University of Cape Town, Cape Town, South Africa;

Howard—School of Geography and the Environment, University of Oxford, Oxford, United Kingdom

Sparrow and Wallom—Oxford e-Research Centre, Department of Engineering Science, University of Oxford, Oxford, United Kingdom;

Li—Environmental Change Institute, and Oxford e-Research Centre, Department of Engineering Science, University of Oxford, Oxford, United Kingdom

CORRESPONDING AUTHOR: Neven Fuckar, neven.fuckar@ouce.ox.ac.uk

This multi-method study of high precipitation over parts of Mozambique, Zimbabwe, and parts of Zambia in February 2018 indicates decreased likelihood of such events due to climate change, but with substantial uncertainty based on the used observations and models.

Precipitation in southern Africa displays a notable zonal gradient (south of about 15°S there is a dominant contrast between dry west and wet east) and is characterized by a pronounced annual cycle as well as high interannual variability (e.g., Lindesay 1988; Nicholson and Kim 1997; Nicholson et al. 2018). During austral summer the complex large-scale monthly precipitation pattern in southeast Africa is strongly guided by the Hadley circulation (Cook 2005) and movement of the associated main tropical cloud and rainband (Schneider et al. 2014; Nicholson 2018), also referred to as the south Indian Ocean convergence zone (Cook 2000; Hart et al. 2010; Barimalala et al. 2018). The main rainband of strongest tropical precipitation reaches the southernmost climatological position across parts of Madagascar, Mozambique, Malawi, Zimbabwe, and Zambia in February (see Figs. ES2 and ES3 in the online supplemental material; Tyson and Preston-Whyte 2002; Reason 2017).

In February 2018, the main tropical rainband moved much farther south and led to anomalous high rainfall over central and southern Mozambique, Zimbabwe, and southern Zambia (Figs. 1a–f and Figs. ES1a–c), which resulted in significant socio-economic impacts in the region (e.g., flooding was reported in parts of Lusaka, Zambia, and floods in Manica province, Mozambique, triggered the country's emergency response). This study addresses whether and to what extent anthropogenic climate change has altered the likelihood of this large-scale high precipitation event in February 2018 to occur by applying a multi-method event

attribution approach (National Academies of Sciences, Engineering, and Medicine 2016; Otto 2017; van Oldenborgh et al. 2019, manuscript submitted to Bull. Amer. Meteor. Soc.).

Event definition and observational results.

First, to establish the spatial extent of the high precipitation event of interest, we use multiple high-resolution gridded satellite-era products. Figures 1a–c (and Figs. ES1a–c) show February 2018 total precipitation in such three analyses commonly used for monitoring of droughts and floods. Furthermore, Figs. 1d–f show the strong positive precipitation anomalies in February 2018, with variable spatial extents in different datasets in subtropical southern Africa (south of 15°S). To get a detailed spatial definition of this large-scale event to envelop the large anomalies in monthly precipitation (above 150 mm), we define the region "MZZ" as encompassing provinces where significant positive anomalies are present in at least two of the satellite-era analyses shown in Figs. 1d–f: Gaza, Inhambane, Manica, and Sofala provinces in Mozambique; all of Zimbabwe; and Southern and Lusaka provinces in Zambia (red contour in Figs. 1d–f), covering about 0.78 M km2.

We utilize three long-term gridded in situ datasets to determine the return time of the February 2018 total precipitation averaged over the MZZ region. February 2018 MZZ precipitation in the Climatic Research Unit (CRU) TS v4.03 (177 mm), the Global Precipitation Climatology Centre (GPCC) v2018 (230 mm), and NOAA's Precipitation Reconstruction over Land (PREC/L) (173 mm) appears to be less intense than in three used satellite-era datasets [Fig. ES1: 333 mm in the Climate Hazards Infrared Precipitation with Stations (CHIRPS2), 284 mm in Tropical Applications of Meteorology using Satellite and Ground−Based Observations (TAMSAT3), and 287 mm in the Tropical Rainfall Measuring Mission (TRMM) 3B43] since it has the 35th rank (out of 118 years), the 15th rank (out of 119 years), and the 21st rank (out of 72 years), respectively. The generalized Pareto distribution (GPD; Coles 2001) is a well-established choice for statistical modeling of extreme occurrences over high thresholds (Davison and Smith 1990). We utilize the GPD as a limiting high-tail distribution of precipitation and in the widest range it is commonly fit in the top 20% of distribution. However, February 2018 MZZ precipitation levels in CRU TS and NOAA PREC/L are just barely in the top 30%, and at these observed levels a more suitable fit is the Gaussian distribution. Hence, to get the return period of this event in CRU TS and NOAA PREC/L (GPCC) we fit a Gaussian distribution (a GPD to the top 20% values) whose parameters scale with a 4-yr smoothed NASA GISS global mean surface temperature (GMST) [for scale fit methodology see, e.g., Philip et al. (2018), Otto et al. (2018a), and the supplement]. Only NOAA PREC/L shows a statistically significant negative linear trend (95% confidence level) of −3.6 mm (0.1°C of GMST)−1 with p = 0.007 (Figs. 1g–i), while it has a temporal trend of −5.2 mm decade−1 with p = 0.012. The mean return time of the event in CRU TS, GPCC, and NOAA PREC/L is 5, 20, and 9 years, respectively (Figs. 1j–l), so for the event definition we use a combined (and rounded) return time of 10 years (i.e., having 10% chance of occurring in a year). The 2018 versus 1901 probability (or risk) ratio in CRU TS and NOAA PREC/L based on a Gaussian scale fit with GMST is 0.63 [95% confidence interval (CI): 0.18, 1.45] and 0.27 (95% CI: 0.08, 0.71), respectively, while in GPCC based on a GPD scale fit with GMST is 0.40 (95% CI: 0.02, 48.68), where the 95% confidence interval is estimated from

1000-member nonparametric bootstrap. This probability ratio (PR) is the ratio between the occurrence probability (reciprocal return time) of the event under 2018 conditions (i.e., today's climate) divided by the occurrence probability under 1901 conditions (i.e., a historical climate approximately close to pre-industrial conditions).

Modeling results.

We use large (≥10 members) and very large (>100 members) ensemble simulations with comprehensive (i.e., general circulation) climate models to assess whether and to what extent anthropogenic climate change modified the likelihood of this event following established methodology (e.g., Philip et al. 2018; van der Wiel et al. 2017; van Oldenborgh et al. 2017). To verify that we are using a suitable model for event attribution we assess whether it can reproduce key statistical aspects of the observed distribution; to that end we focus on the dispersion parameter σ/μ (the standard deviation over the mean) from long-term in situ observations. The value of σ/μ in CRU TS, GPCC, and NOAA PREC/L is 0.41 (95% CI: 0.34, 0.49), 0.44 (95% CI: 0.35, 0.53), and 0.35 (95% CI: 0.27, 0.45), respectively, so we require of models to have the mean dispersion parameter between 0.27 and 0.53 (Fig. ES4). We use as event definition the return period of 10 years in today's climate for a February total precipitation averaged over the MZZ region instead of a specific precipitation level to adjust for mean biases across climate models (e.g., Otto et al. 2018b). In other words, for each model the 10-yr return time corresponds to a slightly different total precipitation level.

First, we use weather@home2 (w@h2)—the regional atmosphere–land model HadRM3P with a southern African domain (50-km resolution) nested in the global atmosphere–land model HadAM3P (CMIP3 generation)—through the distributed computing system climateprediction.net (Guillod et al. 2017). In this study, we utilize 658 members of actual (factual/historic) February 2018 HadRM3P simulations (using observed SST, sea ice, greenhouse gases, and aerosol forcings), and 658 members of natural (counterfactual) February 2018 simulations that uses pre-industrial SSTs and sea ice (Schaller et al. 2016) as well as greenhouse gases and aerosols. The σ/μ value in both actual and natural HadRM3P ensemble simulations is 0.39. Direct comparison of these two ensembles, without using a scale fit with GMST, yields a PR of 1.21 (95% CI: 0.80, 1.83) for the event of interest with the return period of 10 years in 2018 actual climate (Fig. 2a where the 95% CI is estimated by a 1000-member bootstrap).

Then we turn our attention to six fully coupled climate models (CMIP5 and CMIP6 generations), all with adequate σ/μ, and analyze their historical ensemble simulations (see the supplement for model details and Fig. ES4). We fit a GPD that scales with 4-yr smoothed GMST to the top 20% of February MZZ precipitation to obtain the following 2018 versus 1901 probability ratios for the adjusted precipitation levels that match the return time of 10 years in 2018 (Figs. 2b–g):

1) 16 ensemble members of EC-Earth2.3 ($\sigma/\mu = 0.32$): PR = 0.94 (95% CI: 0.27, 2.05).

2) 30 ensemble members of CSIRO-Mk3.6 ($\sigma/\mu = 0.50$): PR = 0.78 (95% CI: 0.51, 1.27).

3) 10 ensemble members of MIROC6 ($\sigma/\mu = 0.38$): PR = 0.74 (95% CI: 0.41, 4.58).

4) 40 ensemble members of CESM1-CAM5 ($\sigma/\mu = 0.41$): PR = 0.68 (95% CI: 0.36, 1.01).

5) 20 ensemble members of GFDL-CM3 (σ/μ = 0.36): PR = 0.66 (95% CI: 0.21, 1.07).

6) 10 ensemble members of CNRM-CM6.1 (σ/μ = 0.48): PR = 0.51 (95% CI: 0.26, 1.48).

Synthesis and conclusions.

We performed a multi-method event attribution using three satellite-based and three long-term station-based monthly precipitation analyses along with seven climate models to examine the change in likelihood of the February 2018 high precipitation averaged over the MZZ region in southern Africa due to anthropogenic forcings. The overall PR result is illustrated by the purple "synthesis" bar in Fig. 2h, which shows the unweighted average (based on geometric means) of 0.63 (95% CI: 0.22, 2.11). The mean PR—indicating that such a high precipitation event has most likely become 37% less probable—is consistent with the expected poleward expansion of the Hadley cells and drying over southern Africa due to the global climate change (e.g., Ma et al. 2018; Munday and Washington 2019); however, the 95% CI of PR is substantial. More specifically, the PR could be ≥1 and thus encompasses the possibility of no significant change or even an increase in the probability of this event. In this attribution study, we do not aim to discriminate between the daily processes leading to such a large-scale monthly event. While extreme precipitation in the MMZ region is sometimes associated with intense tropical cyclones from the Indian Ocean, such as Idai in March 2019 and Eline in February 2000, this was not the case in February 2018, as no tropical cyclones made landfall that month [Météo France Regional Specialized Meteorological Center (MFR/RSMC) La Reunion]. Based on CHRIPS2 daily data February 2018 high total precipitation arose from 12 heavy large-scale daily rainfall events over the MZZ region. Furthermore, an analysis of tropical low tracks (Howard et al. 2019) in the ERA5 (Hersbach et al. 2018) and MERRA-2 (Gelaro et al. 2017) reanalyses shows that about 55% of this high daily precipitation occurred in association with an eastward migration of continental tropical lows into Mozambique during 8–13 February 2018 and 16–22 February 22018.

REFERENCES:

Barimalala, R., F. Desbiolles, R. C. Blamey, and C. Reason, 2018: Madagascar influence on the South Indian Ocean Convergence Zone, the Mozambique Channel Trough and southern African rainfall. *Geophys. Res. Lett.*, **45**0, 112380–112389, https://doi.org/10.1029/2018GL079964.

Chen, M., P. Xie, J. E. Janowiak, and P. A. Arkin, 2002: Global land precipitation: A 50-yr monthly analysis based on gauge observations. *J. Hydrometeor.*, **3**, 249–266, https://doi.org/10.1175/1525-7541(2002)003<0249:GLPAYM>2.0.CO;2.

Coles, S., 2001: *An Introduction to Statistical Modelling of Extreme Values*. Springer, 209 pp.

Cook, K. H., 2000: The South Indian convergence zone and interannual rainfall variability over southern Africa. *J. Climate*, **13**1, 3789–3804, https://doi.org/10.1175/1520-0442(2000)013<3789:TSICZA>2.0.CO;2.

Cook, K. H., 2005: Hadley circulation dynamics: Seasonality and the role of continents. *The Hadley Circulation: Past, Present, and Future*. H. F. Diaz and R. S. Bradley, Eds., Kluwer Academic, 61–83, https://link.springer.com/chapter/10.1007/978-1-4020-2944-8_3.

Davison, A. C., and R. L. Smith, 1990: Models for exceedances over high thresholds (with discussion). *J. Roy. Stat. Soc.*, **52B**, 393–442.

Funk, C., and Coauthors, 2015: The Climate Hazards Infrared Precipitation with Stations—A new environmental record for monitoring extremes. *Sci. Data*, **2**, 150066, https://doi.org/10.1038/sdata.2015.66.

Gelaro, R. W., and Coauthors, 2017: The Modern-Era Retrospective Analysis for Research and Applications, version 2 (MERRA-2). *J. Climate*, **30**4, 5419–5454, https://doi.org/10.1175/JCLI-D-16-0758.1.

Guillod, B. P., and Coauthors, 2017: weather@home 2: Validation of an improved global–regional climate modelling system. *Geosci. Model Dev.*, **10**, 1849–1872, https://doi.org/10.5194/gmd-10-1849-2017.

Hansen, J., R. Ruedy, M. Sato, and K. Lo, 2010: Global surface temperature change. *Rev. Geophys.*, **48**, RG4004, https://doi.org/10.1029/2010RG000345.

Harris, I., P. D. Jones, T. J. Osborn, and D. H. Lister, 2014: Updated high-resolution grids of monthly climatic observations—The CRU TS3.10 dataset. *Int. J. Climatol.*, **34**, 623–642, https://doi.org/10.1002/joc.3711.

Hart, N. C. G., C. J. C. Reason, and N. Fauchereau, 2010: Tropical–extratropical interactions over southern Africa: Three cases of heavy summer season rainfall. *Mon. Wea. Rev.*, **138**, 2608–2623, https://doi.org/10.1175/2010MWR3070.1.

Hersbach, H., and Coauthors, 2018: Operational global reanalysis: Progress, future directions and synergies with NWP. ERA Report Series 27, ECMWF, xxx pp., https://doi.org/10.21957/tkic6g3wm.

Howard, E. R., R. Washington, and K. Hodges, 2019: Tropical lows in southern Africa: Tracks, rainfall contributions and the role of ENSO. *J. Geophys. Res. Atmos.*, https://doi.org/10.1029/2019JD030803, in press.

Huffman, G. J., R. F. Adler, D. T. Bolvin, and E. J. Nelkin, 2010: The TRMM Multi-satellite Precipitation Analysis (TMPA). Satellite Rainfall Applications for Surface Hydrology, F. Hossain and M. Gebremichael, Eds., Springer, 3–22.

Lindesay, J. A., 1988: South African rainfall, the Southern Oscillation and a Southern Hemisphere semi-annual cycle. *J. Climatol.*, **8**, 17–30, https://doi.org/10.1002/joc.3370080103.

Ma, J., and Coauthors, 2018: Responses of the tropical atmospheric circulation to climate change and connection to the hydrological cycle. *Annu. Rev. Earth Planet. Sci.*, **46**, 549–580, https://doi.org/10.1146/annurev-earth-082517-010102.

Maidment, R. I., D. Grimes, R. P. Allan, E. Tarnavsky, M. Stringer, T. Hewison, R. Roebeling, and E. Black , 2014: The 30 year TAMSAT African Rainfall Climatology and Time series (TARCAT) data set. *J. Geophys. Res.*, **119**, 102619–102644, https://doi.org/10.1002/2014JD021927.

Munday, C., and R. Washington, 2019: Controls on the diversity in climate model projections of early summer drying over southern Africa. *J. Climate*, **32**2, 3707–3725, https://doi.org/10.1175/JCLI-D-18-0463.1.

National Academies of Sciences, Engineering, and Medicine, 2016: *Attribution of Extreme Weather Events in the Context of Climate Change*. The National Academies Press, 186 pp., https://doi.org/10.17226/21852.

Nicholson, S. E., 2018: The ITCZ and the seasonal cycle over equatorial Africa. *Bull. Amer. Meteor. Soc.*, **99**, 337–348, https://doi.org/10.1175/BAMS-D-16-0287.1.

Nicholson, S. E., and E. Kim, 1997: The relationship of the El Niño–Southern Oscillation to African rainfall. *Int. J. Climatol.*, **17**, 117–135, https://doi.org/10.1002/(SICI)1097-0088(199702)17:2<117::AID-JOC84>3.0.CO;2-O.

Nicholson, S. E., C. Funk, and A. Fink, 2018: Rainfall over the African continent from the 19th through 21st century. *Global Planet. Change*, **165**, 114–127, https://doi.org/10.1016/j.gloplacha.2017.12.014.

Otto, F. E. L., 2017: Attribution of weather and climate events. *Annu. Rev. Environ. Resour.*, **42**, 627–646, https://doi.org/10.1146/annurev-environ-102016-060847.

Otto, F. E. L., S. Philip, S. Kew, S. Li, A. King, and H. Cullens, 2018a: Attributing high-impact extreme events across timescales—A case study of four different types of events. *Climatic Change*, **149**4, 399–412, https://doi.org/10.1007/s10584-018-2258-3.

Otto, F. E. L., and Coauthors, 2018b: Anthropogenic influence on the drivers of the Western Cape drought 2015–2017. *Environ. Res. Lett.*, **13**2, 124010, https://doi.org/10.1088/1748-9326/aae9f9.

Philip, S., and Coauthors, 2018: Attribution analysis of the Ethiopian drought of 2015. *J. Climate*, **31**, 2465–2486, https://doi.org/10.1175/JCLI-D-17-0274.1.

Reason, C. J. C., 2017: Climate of Southern Africa. *Oxford Research Encyclopaedias: Climate Science*, https://doi.org/10.1093/acrefore/9780190228620.013.513.

Schaller, N., and Coauthors, 2016: Human influence on climate in the 2014 southern England winter floods and their impacts. *Nat. Climate Change*, **6**, 627–634, https://doi.org/10.1038/nclimate2927.

Schneider, T., T. Bischoff, and G. H. Haug, 2014: Migrations and dynamics of the Intertropical Convergence Zone. *Nature*, **513**, 45–53, https://doi.org/10.1038/nature13636.

Schneider, U., A. Becker, P. Finger, A. Meyer-Christoffer, and M. Ziese, 2018: GPCC Full Data Monthly Product Version 2018 at 0.5°: Monthly Land-Surface Precipitation from Rain-Gauges built on GTS-based and Historical Data. Xxxx, https://doi.org/10.5676/DWD_GPCC/FD_M_V2018_050.

Tyson, P. D., and R. A. Preston-Whyte, 2002: *The Weather and Climate of Southern Africa*. 2nd ed. Oxford University Press, 408 pp.

van der Wiel, K., and Coauthors, 2017: Rapid attribution of the August 2016 flood-inducing extreme precipitation in south Louisiana to climate change. *Hydrol. Earth Syst. Sci.*, **21**, 897–921, https://doi.org/10.5194/hess-21-897-2017.

van Oldenborgh, G. J., and Coauthors, 2017: Attribution of extreme rainfall from Hurricane Harvey. *Environ. Res. Lett.*, **12**2, 124009, https://doi.org/10.1088/1748-9326/aa9ef2.

van Oldenborgh, G. J., and Coauthors, 2019: Pathways and pitfalls in extreme event attribution. *Bull. Amer. Meteor. Soc.*, submitted.
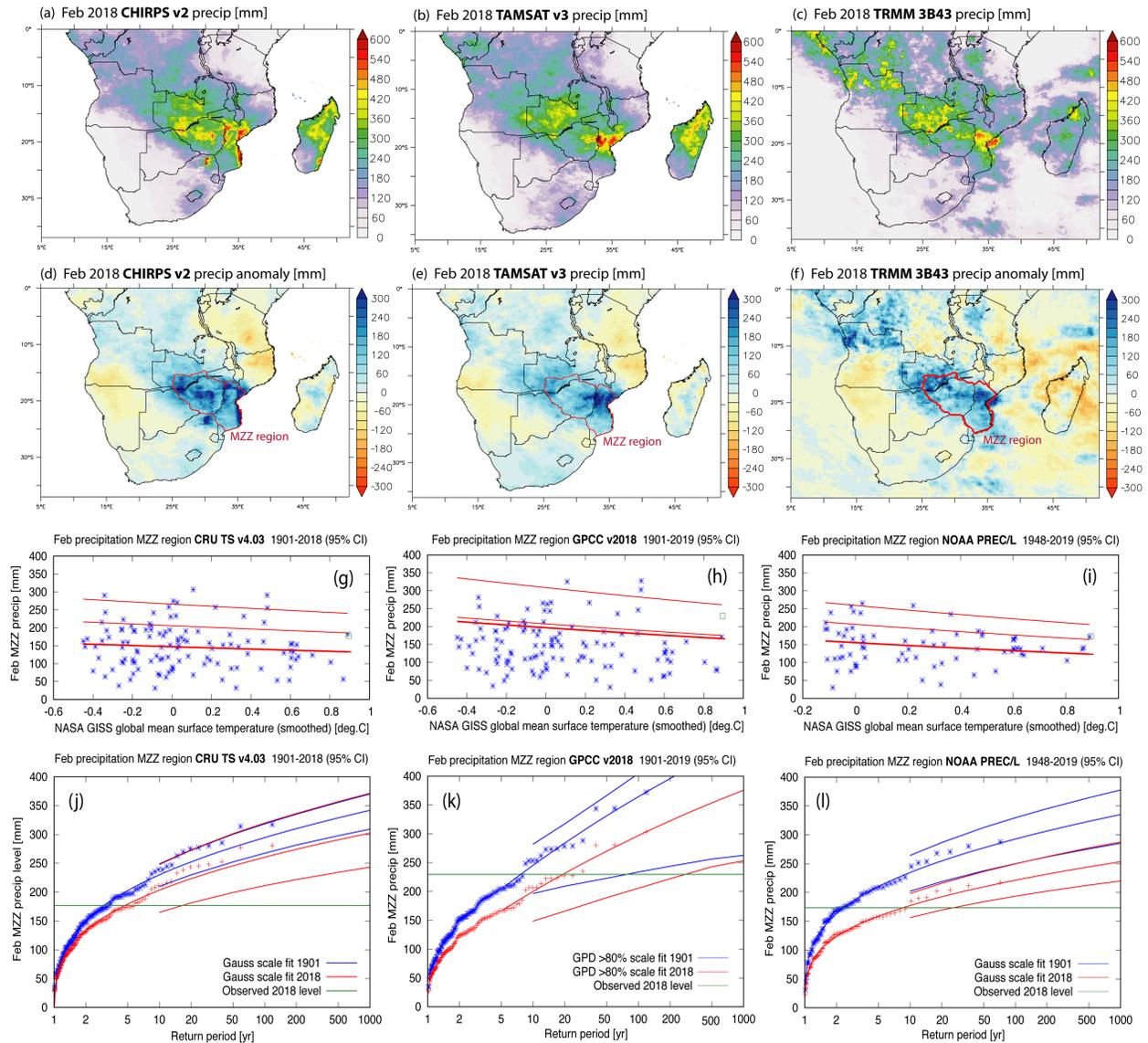
Fig. 1. The top panels show February 2018 total precipitation in the southern Africa from (a) UCSB CHIRPS v2.0 (0.05° resolution, available from 1981; Funk et al. 2015), (b) UR TAMSAT (4-km resolution, available from 1987; Maidment et al. 2014), and (c) NASA TRMM 3B43 (0.25° resolution, available from 1998; Huffman et al. 2010). The second-row panels show the associated February 2018 precipitation anomaly (with respect to the 1998–2018 climatology) from (d) CHIRPS v2, (e) TAMSAT v3, and (f) TRMM 3B43, and outline the MZZ region (red contours). (g)–(i) CRU TS v4.03 (0.5° resolution), GPCC v2018 (0.5°/1° resolution), and NOAA PREC/L (0.5°/1° resolution) February total precipitation averaged over the MZZ region as a function of NASA GISS global mean surface temperature (GMST: Hansen et al. 2010), respectively, and Gaussian or GPD (using the highest 20% values) scale fits. The red lines show fit mean μ, μ+σ, and μ+2σ as function of GMST (4-yr running mean). (j)–(l) The return time plots of February MZZ precipitation with Gaussian, GPD (using the top 20%), and Gaussian scale fits (current/2018 climate in red vs 1901 climate in blue) in CRU TS v4.03 (Harris et al. 2014), GPCC v2018 (Schneider et al. 2018), and NOAA PREC/L (Chen et al. 2002), respectively (green lines show the 2018 event level in different long-term precipitation datasets). The red and blue lines show the mean and 95% confidence interval (CI; based on 1000-member bootstrap) for Gaussian or GPD scale fits.
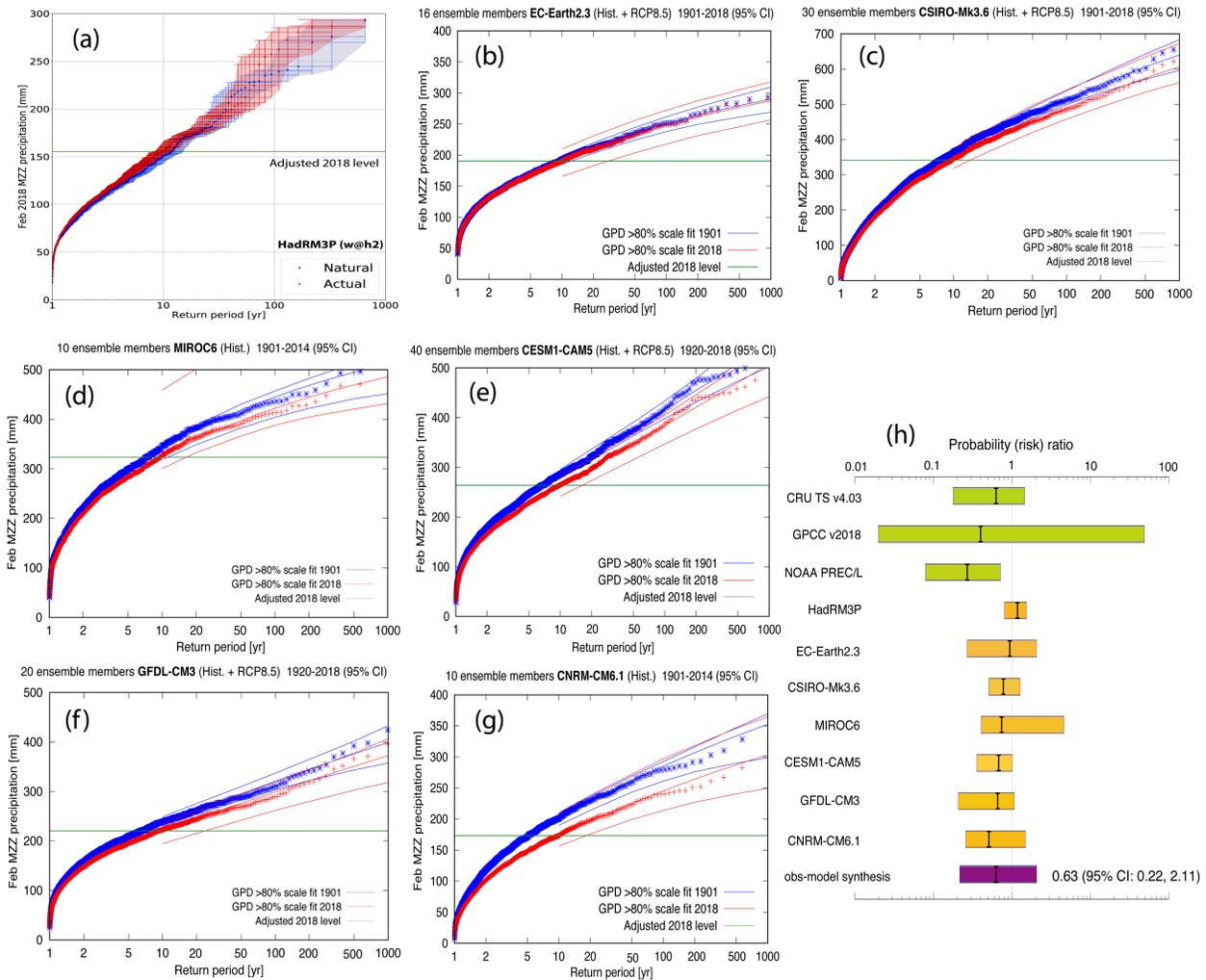
FIG. 2. (a) The return time plot of actual (658 runs) and natural (1749 runs) HadRM3P (weather@home2) simulations for this high total precipitation event in February 2018 averaged over the MZZ region (with 10-yr return time). The red and blue shadings show the 95% CI (based on 1000-member bootstrap). (b)–(g) The return time plots of 16-member EC-Earth2.3 1901–2018, 30-member CSIRO-Mk3.6 1901–2018, 10-member MIROC6 1901–2014, 40-member CESM1-CAM5 1920–2018, 20-member GFDL-CM3 1920–2018, and CNRM-CM6.1 1901–2014 simulations, respectively (a GPD scale fit used the highest 20% of February values to estimate the probability ratios). The red and blue lines show the mean and 95% CI (based on 1000-member bootstrap) for GPD scale fits. (h) Synthesis (purple bar) of the results of our multi-method approach as the probability ratio with 95% uncertainty interval based on the unweighted average (geometric means) of three used long-term observations (lime bars) and seven available climate models (orange bars).